Time-Series Prediction Approaches to Forecasting Deformation in Sentinel-1 InSAR Data

P. Hill [1], J. Biggs [2], V. Ponce-López [1], D. Bull [1]

[1]Department of Electrical and Electronic Engineering, University of Bristol, Bristol, United Kingdom
[2]COMET, School of Earth Sciences, University of Bristol, Bristol, United Kingdom

This manuscript is a preprint and has been submitted for publication in JGR-Solid Earth. It has yet to undergo peer review and the manuscript has yet to be formally accepted for publication. Subsequent versions of this manuscript may have slightly different content.

Time-Series Prediction Approaches to Forecasting Deformation in Sentinel-1 InSAR Data

P. Hill [1], J. Biggs [2], V. Ponce-López [1], D. Bull [1],

[1]Department of Electrical and Electronic Engineering, University of Bristol, Bristol, United Kingdom
[2]COMET, School of Earth Sciences, University of Bristol, Bristol, United Kingdom

Key Points:

- We test established time series prediction methods on 4 years of Sentinel-1 InSAR data, and investigate the role of seasonality.
- For seasonal signals, SARIMA and machine learning (LSTM) perform best over <3 months, and sinusoid extrapolation over >6 months.
- Forecast quality decreases for less seasonal signals, and a constant value prediction performs best for randomly-selected datapoints.

Corresponding author: Paul Hill, `Paul.Hill@Bristol.ac.uk`

Abstract

Time series of displacement are now routinely available from satellite InSAR and are used for flagging anomalous ground motion, but not yet forecasting. We test conventional time series forecasting methods such as SARIMA and supervised machine learning approaches such as Long Short Term Memory (LSTM) compared to simple function extrapolation. We focus initially on forecasting periodic signals and begin by characterising the time-series using sinusoid fitting, seasonal decomposition and autocorrelation functions. We find that the three measures are broadly comparable but identify different types of seasonal characteristic. We use this to select a set of 310 points with highly seasonal characteristics and test the three chosen forecasting methods over prediction windows of 1-9 months. The lowest overall RMSE values are obtained for SARIMA when considering short term predictions (<1 month), whereas sinusoid extrapolation performs best for longer predictions (>6 months). Machine learning methods (LSTM) perform less well. We then test the prediction methods on 2000 randomly selected points with a range of seasonalities and find that simple extrapolation of a constant function performed better overall than any of the more sophisticated time series prediction methods. Comparisons between seasonality and RMSE show a statistically significant improvement in performance with increasing seasonality. This proof-of-concept study demonstrates the potential of time-series prediction for InSAR data but also highlights the limitations of applying these techniques to non-periodic signals or individual measurement points. We anticipate future developments, especially to shorter timescales, will have a broad range of potential applications, from infrastructure stability to volcanic eruptions.

1 Introduction

Many tectonically stable regions suffer from significant ground motion due to the effects of former coalfields (McCay et al., 2018), landslides (Chambers et al., 2008), the shrink and swell of shallow clays (Crilly, 2001; Aldiss et al., 2014), tree growth, coastal erosion, natural sinkholes (Lamont-Black et al., 2002; Banks et al., 1995) and tunnelling (e.g. Crossrail, (Milillo et al., 2018)). Ground motion analysis has recently focused on satellite-based InSAR, which uses the phase difference between pairs of radar satellite images to map ground deformation at mm/yr precision. In particular, the Copernicus Sentinel-1 constellation has revolutionised the coverage, frequency and availability of InSAR data and can be used to produce high resolution maps of ground motion across Europe every six days in near real-time. To this end, many companies have generated post-processed ground motion data maps and time series based on Sentinel-1 InSAR data (*e.g. cgg.com; satsense.com; tre-altamira.com*). Machine learning methods have been used to automatically flag deformation, or changes in deformation in the large datasets (Anantrasirichai et al., 2018, 2019a, 2019b; Gaddes et al., 2019; Valade et al., 2019). Here we investigate the possibility that these Sentinel-1 datasets can be used to forecast future behaviour.

Time series forecasting defines a prediction model to forecast future values of a univariate or multivariate time series based on previously observed values. Time series forecasting plays a significant role in many application domains such as econometrics, mathematical finance, electroencephalography, astronomy and communications engineering. Due to the financial importance of large scale forecasting of commodity values, time series forecasting has been led by disciplines associated with economics. Economic time series forecasting has led to standard time series prediction tools such as SARIMA (Box et al., 2015; Hamilton, 1994; Brockwell & Davis, 2016); a key forecasting tool evaluated within our work. More recently, Recurrent Neural Networks have been effectively used for time series prediction using methods such as LSTMs (Hochreiter & Schmidhuber, 1997; Greff et al., 2017) and sequence to sequence (Seq2Seq) methods (Sutskever et al., 2014; Cho et al., 2014). LSTM and Seq2Seq methods are easily adapted to both univariate or multivariate time series prediction (Rebane et al., 2018; Torres & Qiu, 2018).

For many of the processes that contribute to InSAR measurements, we expect that prior observations will not contain sufficient information to accurately predict future observations. This includes both signals of interest, such as sudden catastrophic failures, and noise terms, such as turbulent atmospheric effects. However, some components of the signal have repeating characteristics, such as multi-year trends and seasonal effects. We begin by analysing the characteristics of the input dataset to select signals with repeating characteristics with a period of 1 year (section 3), and then focus on forecasting over time periods of 1-9 months (section 4 and 5). Finally, we discuss the potential applications and current limitations of time-series forecasting for Sentinel-1 InSAR data.

2 Case Study Dataset

2.1 InSAR Data

We test our algorithms on Sentinel-1 data processed by Satsense Ltd using an algorithm based on the RapidSAR approach (Spaans & Hooper, 2016) (Figure 17). Atmospheric effects are the dominant source of noise in most InSAR datasets and have been reduced within the Satsense data through: (1) The removal of long wavelength signals from each InSAR image using a Gaussian spatial filter. (2) The removal of short wavelength atmospheric signals using an APS (Atmospheric Phase Screen) filter. This isolates the random-in-time effects using a highpass filter and then uses a low-pass spatial filter to estimate the spatially correlated temporally random atmospheric effects. (3) Smoothing the displacemens in time using a per-time-series temporal filter to reduce the effects of overall temporal noise which may include some residual atmospheric noise not removed by the APS filter.

Sentinel-1 acquires data every 6 days over Europe, but due to operational factors, some of this data is missing, particularly in the first year when only Sentinel-1A was operating. Since the algorithms proposed here require regularly sampled data, we interpolate onto an even 6-day temporal grid as shown in Supplementary Figure 1. Simple linear interpolation between neighbours is used to avoid unnecessary assumptions.

2.2 Case Study Area

This project is part of the UK Digital Environment Programme and we use the subsidence of the West Yorkshire coal mines as a case study (Burke et al., 2015; Lake et al., 1992). Here we choose to work on the area around Normanton, which was mined until the mid-1970s and where there is a high density of InSAR scatterers (Figure 1). The area is currently subsiding at a rate of up to 15mm/yr and superimposed on this are seasonal signals, particularly associated with some of the large warehouse buildings in the area.

A subset of the time series (points P1-P8) have been selected for further analysis and forecasting experiments, and these are shown in Figure 1. P1-P3 illustrate the combination of a (downward) trend and seasonality; P4-P6 have a strong seasonal signal, but no long-term trend, and P7 and P8 show trends without seasonality. Points P1-P6 were selected as being the top six seasonal signals according to the analysis in section 3 and points P7 and P8 the lowest. P1-P3 and P6-P7 are car parks; P4 and P5 are the roofs of a house and P8 is the roof of the XPO Logistics warehouse.

3 Seasonal Signals in the InSAR Dataset

3.1 Measures of Seasonality

Our hypothesis is that InSAR signals contain some periodic components, for which time series forecasting may be useful. For this application, we chose to focus on the most common natural periodic variations, those that occur annually. We start by testing the most

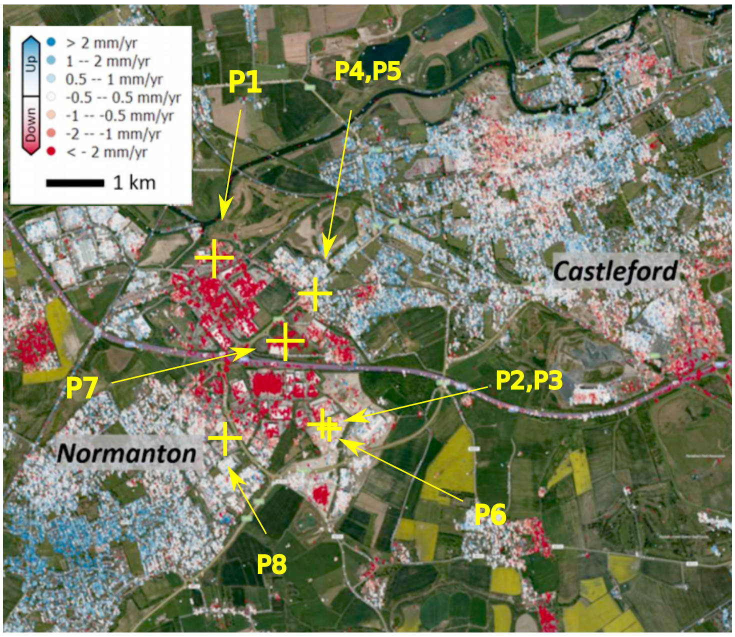

Figure 1. Large scale subsidence in West Yorkshire due to historical shallow coal mining. Central figure shows colour coded motion magnitudes. Points P1-P8 show the chosen points for analysis. P1-P3 illustrate the combination of a (downward) trend and seasonality; P4-P6 have a strong seasonal signal, but no long-term trend, and P7 and P8 show trends without seasonality. P1-P3 and P6-P7 are car parks; P4 and P5 are the roofs of a house and P8 is the roof of the XPO Logistics warehouse. Corresponding time series are shown in Figure 8

commonly used method for estimating and removing seasonal components of geodetic timeseries, namely sinusoid fitting (Watson et al., 2002; Colesanti et al., 2003). However, this measures the correlation with purely sinusoidal behaviour and could potentially exclude periodic signals with other non sinsuoidal but repeating waveforms. First, we review a variety of methods of detecting seasonality (Hartmann et al., 1992; Zubaidi et al., 2018; Hylleberg, 1995) and summarise them in Supp. Table 1. We then focus on methods that are able to generate quantitative measures of annual seasonality rather than simple detection and can be used to analyse pre-defined periods (12 months) rather than estimate the period of seasonality. Based on these criteria, we select 'Seasonal and Trend decomposition using Loess' (STL)(R. B. Cleveland et al., 1990) and autocorrelation function (ACF)(Chen & Boccelli, 2018) for further study. The choice of whether or not to normalise the seasonality measures is a key design decision. With normalisation the amplitude of the seasonality will be disregarded, but if there is no normalisation, high amplitude stochastic signal components will often mask truly seasonal signals with small amplitude. For this reason, all three considered seasonality measures are normalised.

3.1.1 Sinusoid Fitting and Correlation (Sin) Method

We fit a sinusoid of fixed frequency (12 months) to the detrended time series using a least squares method and extract the amplitude and phase parameters. An obvious measure of seasonality is the magnitude of the fitted sinusoid, however, in this case, large magnitude signals that are not particularly seasonal will produce a bigger seasonality index than smaller magnitude signals that are truly seasonal. Instead, we define the seasonal index for this method to be the normalised correlation between the training signal and the fitted sinusoid,

$$\text{SIndex}_{\text{Sin}} = \rho(W_t, \hat{W}_{sin}) \tag{1}$$

where ρ is normalised correlation and $\hat{W}_{sin}$ is the fitted sinusoid.

3.1.2 STL decomposition

The concept of a "seasonal decomposition" of a time series signal means that the time series can be decomposed into a sum (or a product) of three components: a trend, a seasonal component, and a residual. We have used the common implementation of STL as initially described by Cleveland (R. B. Cleveland et al., 1990) assuming an additive STL model. This implementation uses Loess smoothing, which uses iterative sliding window regression to generate smooth functions (seasonal and trend) (W. S. Cleveland, 1979). First Loess smoothing is applied to remove the seasonal component then a separate Loess smoothing is applied to remove the trend. The remaining component is the residual.

A logical measure of the seasonality can then be defined using the ratio of the variance of the residual (L) to the variance of the signal without the trend (L+S). As this ratio increases as seasonality decreases, we define seasonality as follows. $\text{SIndex}_{\text{STL}}$ is mathematically well behaved and varies from 0 to 1.

$$\text{SIndex}_{\text{STL}} = 1.0 - \frac{\text{Var}[L]}{\text{Var}[L+S]} \tag{2}$$

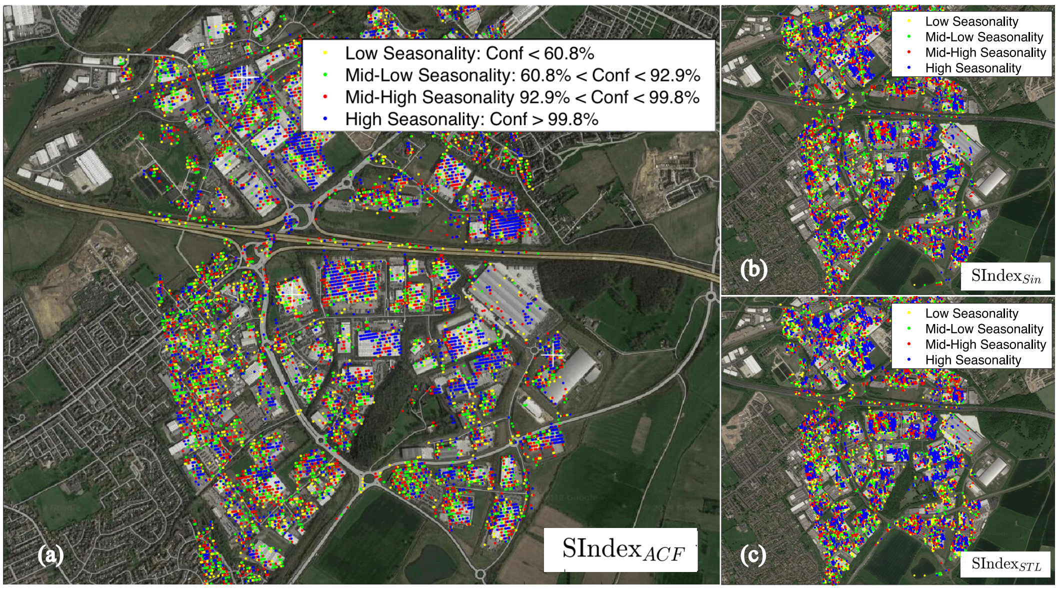

Figure 2. Dataframe of InSAR datapoints in Normanton area grouped by levels of seasonality using; (left) $\text{SIndex}_{\text{ACF}}$, (top right) $\text{SIndex}_{\text{STL}}$, and (bottom right) $\text{SIndex}_{\text{Sin}}$. The $\text{SIndex}_{\text{ACF}}$ sub figure is divided into four ranges of confidence bounds. Confidence is calculated as the rejection of the Null hypothesis that the ACF value is insignificant using the standard errors under the assumption of a Gaussian source (as used by the MATLAB `autocorr` function). Seasonality indices $\text{SIndex}_{\text{STL}}$ and $\text{SIndex}_{\text{Sin}}$ are divided into four equal and sorted ranges of seasonality indexed by colour.

3.1.3 Autocorrelation Function (ACF) Method

The autocorrelation function (ACF) measures how self-similar a signal is by measuring the correlation of the signal with shifted versions of itself (Chen & Boccelli, 2018; Carla et al., 2016). These shifts are known as lags and in this case, we are only interested in the lag corresponding to 12 months. As the InSAR signal is sampled every 6 days (from 2015 to 2018) the lag is set to be 60. $\text{SIndex}_{\text{ACF}}$ is well behaved and varies from 1 (perfect correlation) to -1 (perfect anti-correlation). It is defined in (3) where ρ is the normalised ACF function (with lag 60).

$$\text{SIndex}_{\text{ACF}} = \rho_{60}(W_t) \tag{3}$$

In order to properly estimate seasonality, isolated from the influence of trend, the trend is removed by fitting a second degree polynomial to the InSAR time series and subtracting it when using the ACF method. A second-degree polynomial was chosen to properly model DC variations over the trained signal (this is not done for the STL method where the trend is extracted independently). Confidence values can then be calculated as the rejection of the null hypothesis that the ACF value is insignificant using standard errors under the assumption of a Gaussian source.

3.1.4 Comparison of seasonality measures

For the ACF method (Figure 2(a)), seasonality correlates well with land use type, with the highest values attributed to the roofs of particular buildings (for example the Wakefield ASDA distribution centre). Figures 2(b) and 2(c) show that sinusoid fitting and STL methods are less spatially correlated (in terms of the different seasonality magnitudes) when compared to the ACF based measure.

Figure 3 shows a comparison of the seasonality measures $\text{SIndex}_{\text{Sin}}$, $\text{SIndex}_{\text{STL}}$ and $\text{SIndex}_{\text{ACF}}$ for all the datapoints in Normanton region (with points P1-8 labelled). The approximately linear relationship between the measures demonstrates that they are broadly comparable, and the points P1-6 are classified as highly seasonal by all three indices, whereas P7-8 lie with the majority of points which are not seasonal. However, there is considerable scatter showing that the three indices identify different types of seasonality, with especially large differences between the ACF and STL measures. We use the ACF measure for the subsequent experiments.

4 Ground Motion Forecasting

The task of forecasting InSAR time series can be approached in one of three ways: 1) Future displacements forecast on each point individually, using only information from that point (Mazzanti et al., n.d.); 2) Future displacements can be forecast for each point individually, using the time series itself and a selected group of related time series; 3) Groups of time series can be forecast in a multidimensional sense (Rebane et al., 2018; Torres & Qiu, 2018). For this proof-of-concept, we have focused on the first two approaches for simplicity.

In this paper, we evaluate the forecasting methods by dividing each signal into a "training" sub-range and a contiguous "testing" sub-range in order to be able to generate objective evaluations of each forecast. That is, given an entire temporal signal of T datapoints $W = \{w_1, w_2, ..., w_T\}$, we define "today" as being timestep $= t$ and our goal is to predict a new signal $\hat{\boldsymbol{y}} = \{\hat{w}_{t+1}, \hat{w}_{t+2}, ..., \hat{w}_{t+N_y}\}$ as similar as possible to the original sub-signal $y = \{w_{t+1}, w_{t+2}, ..., w_{t+N_y}\} \in W$. We also define the training set as $W_t = \{w_1, w_2, ..., w_t\} \in W$. The value N_y is a positive scalar integer which determines the period of time to be forecast - i.e. the number of future observations. We set N_y to approximately 9 months (264 days) for all experiments, but evaluate the predic-

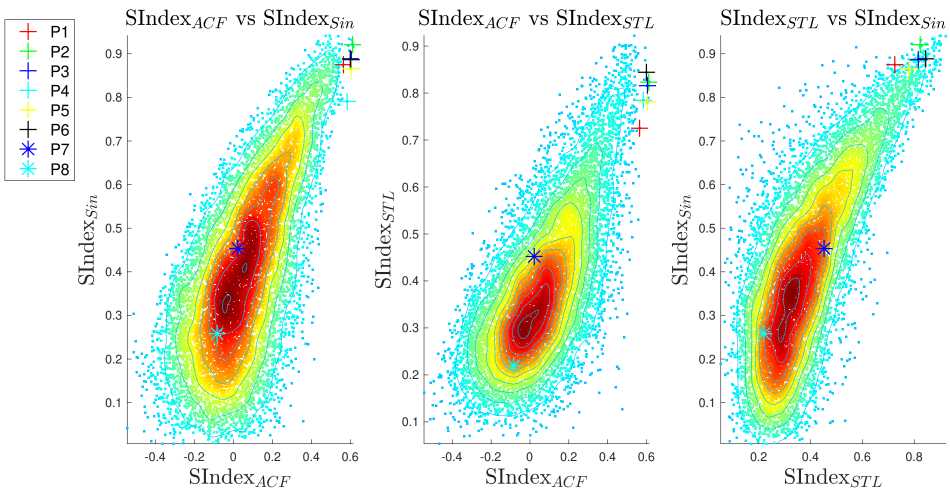

Figure 3. Comparison of Seasonality Measures SIndex$_{\mathrm{Sin}}$ is the normalised correlation between the signal and the best-fitting sinusoid. SIndex$_{\mathrm{STL}}$ is based on a seasonal decomposition (STL) and defined as defined using the ratio of the variance of the residual (L) to the variance of the signal without the trend (L+S). SIndex$_{\mathrm{ACF}}$ is the normalised autocorrelation function with a period of 1 year (or 60 datapoints)

tion over time periods of 1-9 months. The value N_x is a positive scalar integer which determines the period of time for training i.e. the number of past observations. An illustrative example of the predicted and test signals is shown on the right of Figure 4.

A summary of all the forecast methods compared is given in Table 1. In order to compare the SARIMA and LSTM approaches with previously used methods, we include a standard sinusoid fitting algorithm (Watson et al., 2002), and project the fit forward in time. A sinusoid and trend are fitted to the same part of the each of the time series as used for training the other methods (i.e. W_t) and future values extrapolated using the resulting parameterisation.

4.1 Long Short-Term Memory (LSTM) Networks

A Long Short-Term Memory (LSTM) (Hochreiter & Schmidhuber, 1997; Greff et al., 2017) network is a Recurrent Neural Network (RNN) (Rumelhart et al., 1986) architecture used in the field of deep learning for time series data. RNNs keep track of arbitrary long-term dependencies in the input sequences, and they can scale to much longer sequences than classical networks. They are designed to process sequences of variable lengths, where parameters are shared with all previous output members. LSTMs have the ability to add or remove information to a temporal learning "state". This is carefully regulated by structures called gates. The learning selectively *keeps* some part of the past (using the temporal states) and *forgets* others (using "forget" gates). LSTMs are commonly used for classification applications. However, within this application we are using them within the regression framework illustrated in Figure 4 where the output of the network $\hat{y}$ is an array of length N_y.

Table 1. Summmary of Forecasting Methods. For all methods $N_x = 9$ months, $N_y = 9$ months

Method	Definition
Constant	A constant value prediction, taking the last value of the training time series and extrapolating it for the whole of the test series.
Sinu	Sinusoid fitting method: A simplex gradient descent method was used to fit the amplitude and phase of a sinusoid to the data (together with the slope of a linear trend term).
SARIMA	SARIMA based prediction with parameters obtained using the “auto sarima” method (Hyndman et al., 2007).
LSTM1	Single signal used for prediction (based on the univariate method illustrated in Figure 4). Architecture included: two LSTM layers (first with 256 nodes and second with 128 nodes). The final state output of the second LSTM layer is connected to a dense layer of 128 nodes and then subsequently connected to an output layer with N_y nodes. Dropout of level 0.5 is included between each layer, the activation function was ReLU, the loss was MSE, the optimiser was ADAM.
LSTM2	The six most seasonal signals (seasonality measured using $\text{SIndex}_{\text{ACF}}$) concatenated and used for training (Figure 5). The remaining architectural features for this as per LSTM1.
LSTM3	The top 1% of the seasonal signals (seasonality measured using $\text{SIndex}_{\text{ACF}}$) concatenated and used for training as per LSTM2.
LSTM4	The eight spatially closest time series signals (see Supp. Figure 1b) are formed into different features in the multivariate learning process (with a single dimensional feature predicted for the considered time series).
Seq2Seq1	Seq2Seq architecture. The encoder was a single encoder LSTM layer (with 200 nodes) whose output was copied N_y times. This time distributed output was then input into the decoder; a single LSTM layer (with 200 nodes). This was then input to a fully connected dense layer with a final single (but time distributed output layer) node. No dropout was used. The remaining aspects of this architecture were as per LSTM1.
Seq2Seq2	Same as LSTM2 but with Seq2Seq architecture as described for Seq2Seq1.
Seq2Seq3	Same as LSTM3 but with Seq2Seq architecture as described for Seq2Seq1..
Seq2Seq4	Same as LSTM4 but with Seq2Seq architecture as described for Seq2Seq1.

4.1.1 Univariate LSTM: LSTM1

Figure 4 shows the univariate case of forecasting ground motion using a supervised LSTM network. A sliding window forms a training data frame (for a single signal) of inputs ($\mathbf{X}$) and outputs ($\mathbf{Y}$) to train the network. Once trained, the testing input ($\mathbf{X_{test}}$) is ingested into the network to generate the forecast $\hat{y}$ approximating the true sequence y. This requires a final layer in the network to generate a vector the same length as y. This is done using a fully connected dense layer without any subsequent pooling as illustrated in Figure 5. For all the subsequent experiments N_x and N_y are set to 9 months (264 days). This was considered to be long enough to characterise the seasonal nature of the signals, be able quickly to adapt to changes and also have the maximum amount of training data from the sliding window. We use a network of two LSTM layers fully connected to a dense

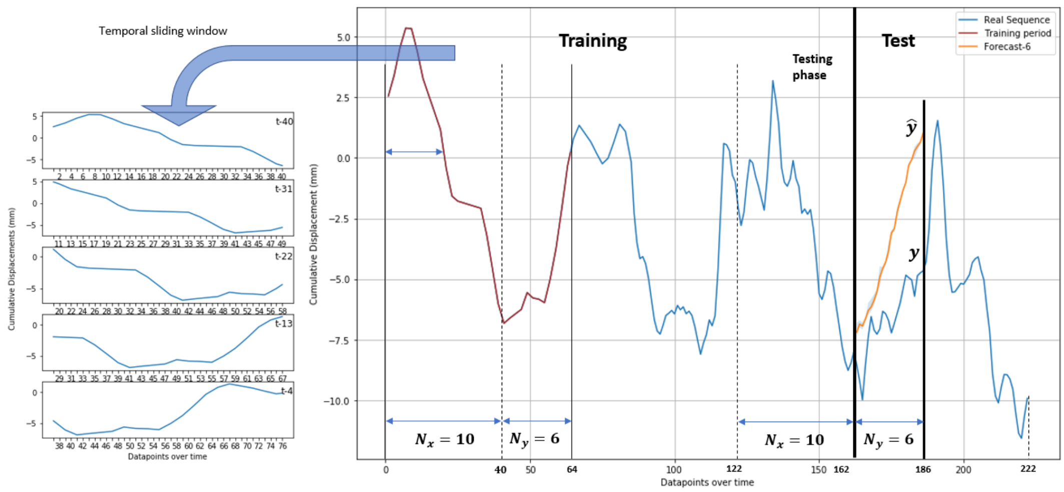

Figure 4. Example of a multi-step approach for time-series forecasting. The considered signal is split into training and test sets. The training set contains the observable data and the test signal $\boldsymbol{y}$ represents the future observations in the test set. This test signal is to be compared with the predicted signal $\hat{\boldsymbol{y}}$ obtained by our method as well as its associated prediction error. Our multi-step approach for LSTMs reframes the whole training data into temporal sliding windows of sizes N_x and N_y for past and future observations, respectively.

layer outputting the N_y regression outputs. Each layer has an integrated dropout function (set to a dropout factor of 0.5 to prevent overfitting). The optimisation was based on the ADAM method (Kingma & Ba, 2015) and Mean Square Error (MSE) as the loss function. We train our networks using 2000 iterations (epochs) to achieve convergence.

4.1.2 Multi-Signal LSTM: LSTM2-4

We adapt the univariate approach shown in Figure 4 to include data from a set of training signals. This multi-signal LSTM is illustrated in Figure 5. This system uses the same network structure as above but vertically concatenates all of the sliding window data from a set of training signals. The testing data remains the same. The LSTM2 system uses the top six seasonal signals for training. The LSTM3 system uses the top 1% of the seasonal signals (using the $\text{SIndex}_{\text{ACF}}$ method) for training. Conversely, LSTM4 uses the eight spatially closest time series signals as features in an eight-dimensional multivariate LSTM input. A multivariate LSTM architecture is then used to generate a univariate forecast from the multivariate InSAR derived ground motion time series data.

4.1.3 Seq2Seq LSTMs: Seq2Seq1-4

Sequence to sequence (Seq2Seq) is an encoder-decoder deep learning architecture for making multi-step predictions (Sutskever et al., 2014; Cho et al., 2014). The previous methods (LSTM1-4) generated the prediction vector using the single output of an LSTM layer together with dense and fully connected layers (with a final vector regression output). Seq2Seq methods have an independent encoder that analyses the input time sequence and generates a characterising set of states that are subsequently input into the decoder. We have used a single LSTM layer as the encoder that outputs the LSTM states of the input time series data as an initial stage. These output states are then copied multiple times (with the number of copies being the required length of the prediction vector output). These copies then form a multidimensional time series input to a decoder (another

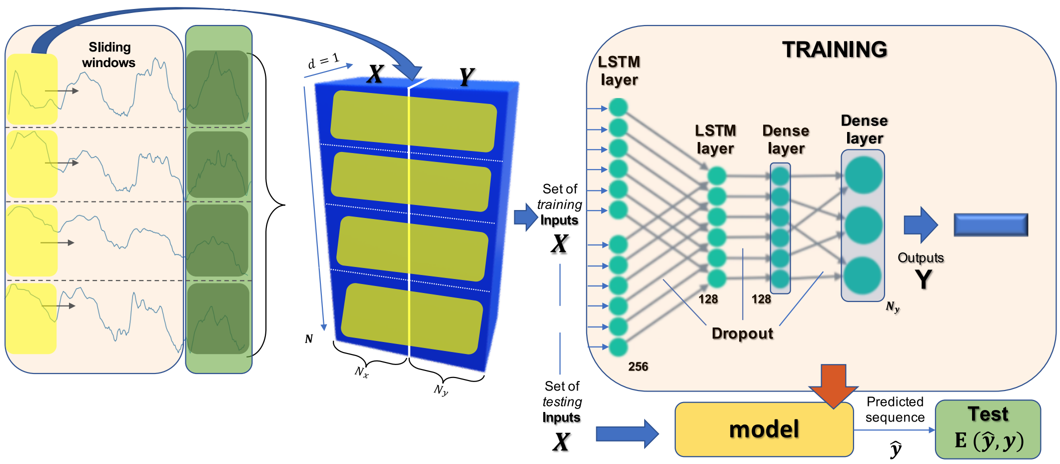

Figure 5. Multi-Signal LSTM. Every signal in the training set is split into training and test sets in the multi-signal approach. First, we use the training sets to frame every signal as a supervised machine learning problem, constructed by a set of inputs $\boldsymbol{X}$ and outputs $\boldsymbol{Y}$. Each considered time-step for the sliding window for each signal becomes a sample in the feature space of input $\boldsymbol{X}$ and output $\boldsymbol{Y}$ of the network.

single LSTM layer). The time distributed outputs are then input into time distributed dense layers outputting a vector forecast result $\hat{y}$. Each method LSTM1-4 has been modified to include a Seq2Seq architecture to form methods Seq2Seq1-4 respectively i.e. the other architectural forms and input/output data structures are equivalent for these two sets of methods.

4.2 SARIMA

SARIMA is an analysis and prediction method for time series data (Box et al., 2015; Hamilton, 1994; Brockwell & Davis, 2016). It is used to model non-stationary data series, where the data are not statistically consistent across time e.g. mean and variance varies with time. It is an analysis tool primarily used to model economic data and is able to identify, model and predict both trend and seasonality (and their variations) over time. SARIMA consists of two sets of forecasting models: trend and seasonality. Each of these two models are divided into three submodels: an autoregressive model (AR) and a Moving Average (MA) model in order to model time variations ("tendencies"). The MA model is the equivalent of an estimated Finite Impulse Response (FIR) filter that just weights recent inputs to combine into an estimated output. Conversely, the AR model is an estimated all-pole or Infinite Impulse Response Filter (IIR) that uses a feedback loop to estimate output given a weighted sum of previous outputs. The input is often further locally differenced (the I stage) to model changes in offset (the third submodel).

The model is comprised of these three sub-models (AR, MA and I) estimated directly on the data to model trend but also over a set lag directly related to the seasonality of the signal. A SARIMA model is then defined as the order of these six models (plus the analysis seasonality lag m):

where p is the order of the AR term, q is the order of the MA term, d is the number of differencing operations required to make the time series stationary, P is the order of the AR seasonality term, Q is the order of the MA seasonality term, D is the num-

$$\text{SARIMA} \quad \underbrace{(p,d,q)}_{\substack{\uparrow \\ \text{Non-seasonal part} \\ \text{of the model}}} \quad \underbrace{(P,D,Q)_m}_{\substack{\uparrow \\ \text{Seasonal part of} \\ \text{of the model}}}$$

ber of differencing operations required to make the seasonal time series stationary and m is the seasonality lag.

The parameters of the SARIMA model are commonly not estimated automatically i.e. the statistics and correlation of the time series signal is analysed by hand and the parameters are tuned until the signal (when compensated by the found parameters) is considered to be stationary. However, recent automatic parameter estimation methods do a minimisation search on some training data to determine the best combination of SARIMA parameters (Hyndman et al., 2007). This method estimates the stationarity of the signal under the parameters and specifically uses the Akaike Information Criterion (AIC) and the Bayesian Information Criterion (BIC) estimators to compare models. The lower these values, the better the model fits the data (Hyndman et al., 2007).

Here, SARIMA parameters are fitted to the training data using Hyndman's method (Hyndman et al., 2007). A typical model for the analysed InSAR time series below was SARIMA$(3,0,2)(1,1,0)_{60}$. The parameters are estimated using the same part of each of the time series as used for training with LSTMs (i.e. W_t) and then SARIMA is used to predict the same part of each time series as with LSTMs (i.e. W_y).

5 Forecast Performance

5.1 Seasonal Signals

We test the forecasting performance of LSTMs and SARIMA on a set of 310 highly seasonal signals selected using the $\text{SIndex}_{\text{ACF}}$ metric. We benchmark the results against sinusoid extrapolation and a constant value prediction. To assess the performance of each model, we use the Root Mean Square Error, $RMSE(\hat{\boldsymbol{y}})=\sqrt{\boldsymbol{E}((\hat{\boldsymbol{y}}-\boldsymbol{y})^2)}$ (Figures 6, 7). We also consider normalised RMSE and define n1RMSE and n2RMSE as the RMSE of the prediction normalised against the variance and constant value prediction respectively (Supp. Figures 2-5). The RMSE distributions are displayed in the form of a boxplot that includes the quartiles of the distribution (the middle line in each box is the distribution median).

For a one month prediction (Figure 6a), the best performing methods were SARIMA and LSTM3, which performed marginally better than the constant value prediction. Of the Seq2Seq methods, the best performers were the univariate version Seq2Seq1 and Seq2Seq4, which was trained with using the 8 geographically closest points. For these short time periods, the sinuoidal extrapolation method (Sinu) performed poorly, with a median RMSE value considerably higher than that of the constant value prediction. Conversely, for longer time periods (Figure 6b), the best performing method was sinusoid extrapolation, with a median RMSE value about 75% of the constant value prediction. The best performing LSTMs were LSTM3 and LSTM4, while Seq2Seq1 and Seq2Seq4 continue to outperform the multi-signal Seq2Seq methods (Seq2Seq2-3). Over these time periods, most of the methods outperformed the constant value prediction, with only LSTM2, Seq2Seq2 and Seq2Seq3 performing worse (when considering median value of n2RMSE: Supp. Figure 3).

For all the time periods considered, the multi-signal Seq2Seq models (Seq2Seq2-3) trained using a set of seasonal signals performed worse than the univariate case (Seq2Seq1).

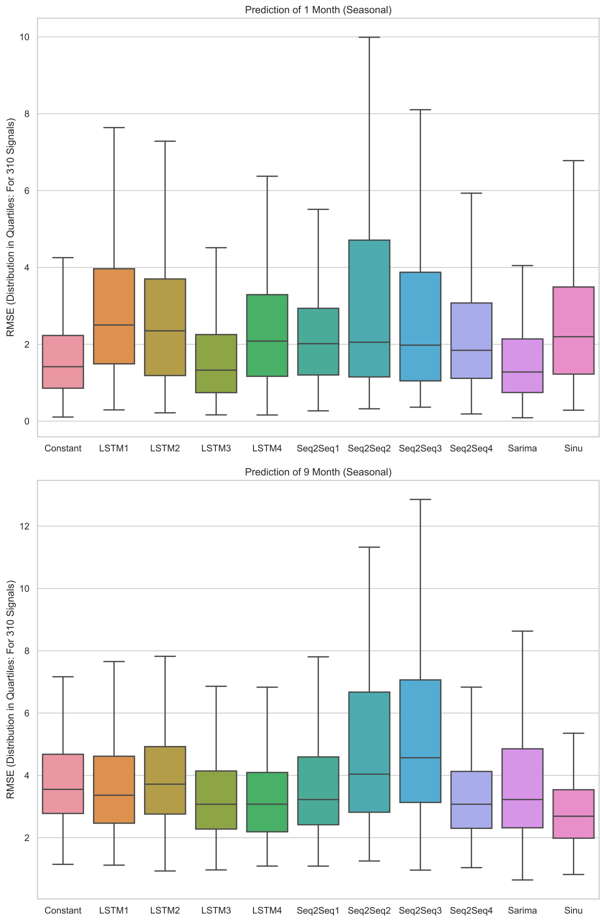

Figure 6. Forecast performance on seasonal signals. The boxplot lines represent the quartiles of the RMSE distribution for all 310 signals with coloured area being the central two quartiles and the central line being the median. a) performance over 1 month; b) performance over 9 months.

We conclude that any improvements gained by having a larger training dataset are offset by the potentially unrelated data statistics and characteristics. However, Seq2Seq4, which was trained using geographically close signals, performed as well as, or a little better than, the univariate case (Seq2Seq1) suggesting that geographically close points have more similar signals, as for example, they may be located on the same structure.

Based on this assessment, we select LSTM3, Seq2Seq4 and SARIMA for further analysis and some examples of the predicted and real timeseries are shown in Figure 8. Points P1-P6 were selected as they have the most seasonal characteristics signals as defined by $\mathrm{SIndex}_{\mathrm{ACF}}$. All methods capture some aspects of the signal, and the timeseries plots are helpful in identifying sources of misfit. For example, sinusoid extrapolation is a global fitting method, so there is often a discontinuity between the training and prediction data (e.g. P3, P6; Figure 8), which explains why the RMSE is high when short prediction periods are considered (Figure 6a). Similarly, the SARIMA results can be seen to characterise the sub-seasonal variations of many of the example 6 signals, but for P1 and P2, the trend has not been accurately estimated and the prediction, although plausible in shape, has an inaccurate offset.

The results in Figure 6 suggests that performance varies according to prediction window, so we test the selected methods over periods of 1-9 months and compare the distribution of RSME values (Figure 7). The lowest RMSE values are obtained for SARIMA when considering short term predictions of < 3 months, whereas sinusoid extrapolation

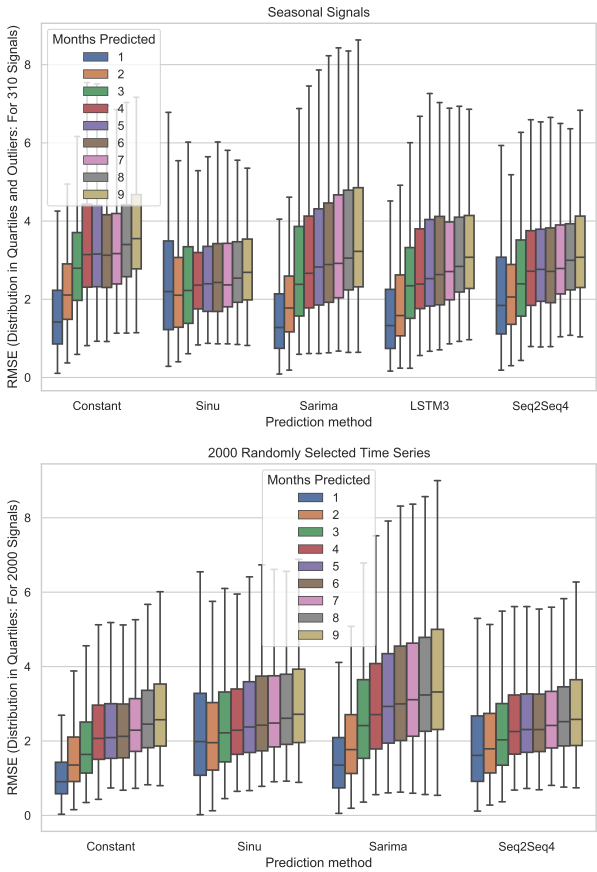

Figure 7. Forecast performance according to prediction window for a) 310 seasonal signals and b) 2000 randomly-selected signals. The boxplot lines represent the quartiles of the RMSE distribution with coloured area being the central two quartiles and the central line being the median.

performs best for predictions of > 6 months. As expected RMSE increases with increasing prediction window: the constant value prediction has a median RMSE value of 1.4 cm for a 1 month window, increasing to 3.6 cm for a 9 month window. Normalising the RMSE to the RMSE value of the constant value prediction (n2RMSE, Supp. Figure 5) removes this effect, and shows that SARIMA and Seq2Seq4 outperform the constant value prediction for all windows, whereas Sinu and Seq2Seq4 only perform better when forecasting 3 or more months into the future.

The multi-signal LSTM (LSTM3) gave the best results for short term prediction (< 3 months). SARIMA also gave good results for short term prediction but gave significantly worse results (compared to LSTM3) for predicting many months into the future. The performance of the Seq2Seq4 method was virtually identical to the LSTM3 method for a period of 9 months but had a slightly larger median error (by 0.3cm) for 1 month.

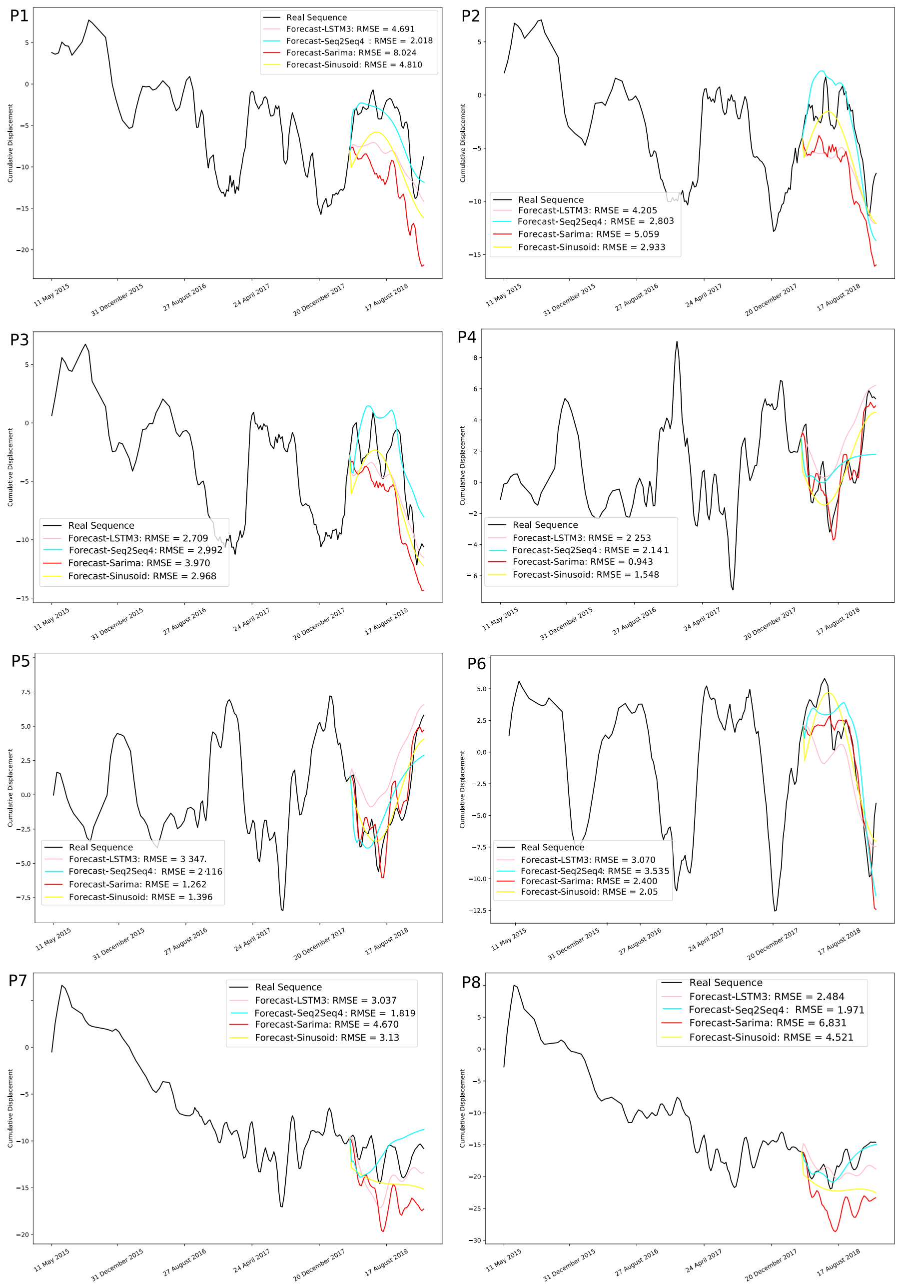

Figure 8. InSAR example forecasts of eight sample signals: LSTMs, SARIMA and Sinusoid Fitting. $N_y = 9$ months ($N_x = 9$ months for LSTMs). The top six signals are highly seasonal signals whereas the bottom two are highly un-seasonal

5.2 Randomly Selected Signals

Finally, we select 2000 points at random from the Normanton dataset with no regard to seasonality and test the methods that performed best on the seasonal signals: SARIMA and Seq2Seq4. We no longer consider LSTM3 since it was trained specifically on highly seasonal signals. Points P7-P8 shown in Figure 8 illustrate the challenges of time-series prediction for non-seasonal signals. Figure 7 shows that the relative variation in RMSE with prediction window is similar to that for seasonal signals. However, this figure shows that none of the methods perform better than the constant value prediction when signals are randomly selected (see also Supp. Figure 5).

Figure 9 shows the relationship between forecast performance (RMSE) and seasonality ($\mathrm{SIndex}_{\mathrm{ACF}}$) for a prediction window of 9 months for the Seq2Seq4, SARIMA and Sinu Methods. For Seq2Seq4, the forecast performance appears independent of seasonality, whereas the SARIMA and Sinu methods perform better (decreased RMSE) with increased seasonality. To test the statistical significance of this relationship, we set the null hypothesis (H_0) that the slope of the regression line is zero and the test hypothesis (H_1) that the slope of the regression line is negative. The p-values of the standard linearity test are 0.0014; 7.6×10^{24} and 3.9×10^{31} for Seq2Seq4, SARIMA and Sinu respectively. These values all exceed a significance threshold of 0.001. There is a clearly statistically significant decrease in RMSE with an increase of $\mathrm{SIndex}_{\mathrm{ACF}}$ for SARIMA and Sinu, while the relationship is close to the significant limit for Seq2Seq4. A similar pattern is seen for all prediction windows (Supp. Figure 6).

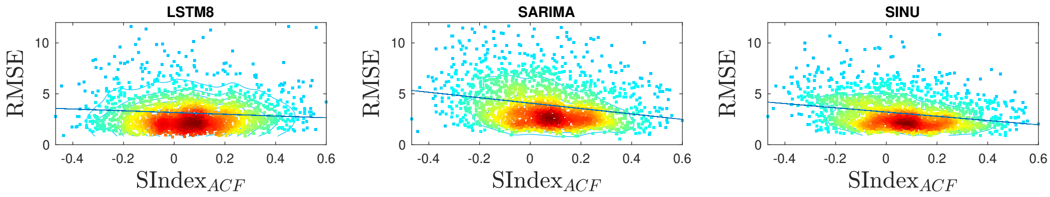

Figure 9. RMSE vs Seasonality Seq2Seq4, SARIMA and Sinu Methods. Plots show are for prediction windows of 9 months, with full results for predictions windows of 1-9 months shown in Supp Figure 6.

6 Discussion

Previous studies have reported annual variations in InSAR data associated with processes such as tropospheric water vapour (Heleno et al., 2010), thermal contraction and expansion (Lazecky et al., 2016), ground water (Bell et al., 2008) and freeze-thaw cycles (Daout et al., 2017). We find that our dataset from the Normanton area of the United Kingdom also contains signals with periodic variations, the strongest of which are clustered on large warehouses suggesting the dominant effect here is thermal expansion and contraction of man-made structures.

We test the ability of a range of established time series prediction methods to forecast InSAR time series and find that several methods perform better than a constant value prediction when signals dominated by periodic variations are considered. The lowest RMSE values are obtained for SARIMA when considering short term predictions (<3 months), whereas sinusoid extrapolation performs best for longer predictions (>6 months). However, for non-seasonal signals, the simple extrapolation of a constant function perform better overall than any of the more sophisticated time series prediction methods. Comparisons between seasonality and RMSE show a statistically significant improvement in performance with increasing seasonality, which suggests pre-processing should be used to select appropriate points before time-series prediction is applied.

The metrics used only compare the global distribution of RMSE values, but the breadth of the distribution and scatter of outliers shows that the misfit is highly variable between observation points, even when seasonality is taken into account. Thus, if a prediction for a single observation point is required, there may be a large misfit in the prediction even for the best performing approaches, but a poorly performing method might produce a very accurate prediction.

The machine learning methods (LSTM and Seq2Seq) tested performed well in some cases, with the use of multivariate or concatenated signals improving the performance. However, it is interesting that they performed less well overall than simple extrapolation of a constant value (for non-seasonal signals) or a sinusoid (for seasonal signals). Interestingly, the performance of the machine learning methods only improved slightly with increasing seasonality, suggesting that they are failing to capture the periodic component of the signal, perhaps because they are only trained over 9 months. Poor performance in predicting financial time series using LSTMs has also been reported (Sirignano & Cont, 2019). This is assumed to be related to the non-stationary nature of the data and the inability of LSTMs to model feedback effectively. Improvements in prediction using LSTMs should follow through both large increases in training data (number of data sequences and length of sequences) together with the integration of SARIMA type feedback modelling.

In this study, we have focused on predictions for windows of less than the period of the signal (1 year), but both SARIMA and sinusoid extrapolation are able to predict for an arbitrary amount of time into the future. Figure 10 demonstrates that predictions for several years into the future show plausible time series, but unfortunately, no quantitative evaluation is possible until a longer dataset of measurements is acquired. Similarly, LSTM methods require a training window that is at least as long as the prediction window, and will require longer timeseries before long-term predictions can be tested.

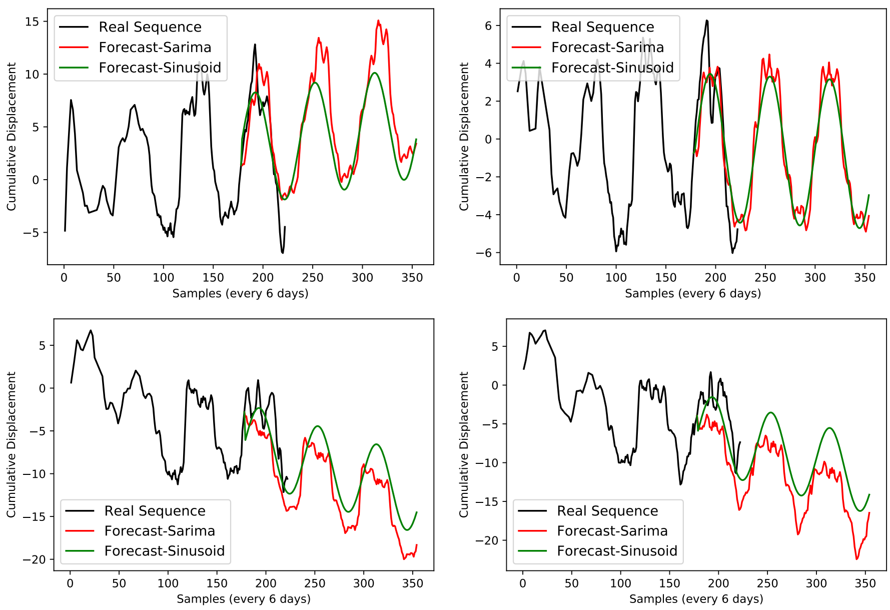

Figure 10. InSAR example forecasts of seasonal signals (far into the future: 3 years)

Real-time monitoring and ground motion forecasting of periodic signals from InSAR data could be used in one of two ways. The first of these is to predict seasonally varying ground motion signals that could otherwise obscure subtle deformation changes that could be pre-cursors to rapid and critical collapses (Selvakumaran et al., 2018). In this case, the reduction in background noise could enable the detection of anomalous or unexpected behaviour. Alternatively, the periodic motion itself is of interest to insurance companies looking to forecast claims due to ground cracking and subsidence (Crilly, 2001), or bridge motion (Lazecky et al., 2016). The broad distribution of misfit values suggests these approaches will only be useful when considering the distribution of a large number of datapoints, and the probability of a good prediction for any single observation point is quite small.

This is a proof-of-concept study and the methods described here can be further refined. Possible future directions include testing different neural network architectures including convolutional LSTMs and attention based systems; the combination of SARIMA and LSTMs; the integration of spatial analysis using CNNs and multivariate prediction using Vector Autoregression. Future developments in machine learning and artificial intelligence may improve performance, but the lack of periodic or repeating signals within the dataset may always be a barrier to time series prediction.

7 Conclusion

In this proof-of-concept study, we have tested a range of time series prediction tools on ground motion data collected using InSAR. For randomly-selected data, a simple constant value prediction outperforms both conventional time series analysis and forecasting methods such as SARIMA and supervised machine learning approaches such as LSTMs. This reflects the stochastic nature of the signals and the difficulties in using any trained system to predict far into the future. The time series prediction methods performed better on signals containing strong annual variations, and both LSTM based architectures and SARIMA performed better over short periods of time (less than three months) than the extrapolation of a sinusoidal function. This suggests that a pre-processing step could be used to select signals that are suitable for forecasting. However, further developments in machine learning and artificial intelligence will be needed before time series predictions of InSAR data are sufficiently reliable to be used in practice.

8 Acknowledgements

We thank SatSense Ltd for access to their dataset over the Normanton/Castleford area. This work was funded by the Digital Environment Programme under NE/S016104/1.

References

Aldiss, D., Burke, H., Chacksfield, B., Bingley, R., Teferle, N., Williams, S., ... Press, N. (2014). Geological interpretation of current subsidence and uplift in the london area, uk, as shown by high precision satellite-based surveying. *Proceedings of the Geologists' Association*, *125*(1), 1–13.

Anantrasirichai, N., Biggs, J., Albino, F., & Bull, D. (2019a). The application of convolutional neural networks to detect slow, sustained deformation in insar time series. *Geophysical Research Letters*, *46*(21), 11850–11858.

Anantrasirichai, N., Biggs, J., Albino, F., & Bull, D. (2019b). A deep learning approach to detecting volcano deformation from satellite imagery using synthetic datasets. *Remote Sensing of Environment*, *230*, 111179.

Anantrasirichai, N., Biggs, J., Albino, F., Hill, P., & Bull, D. (2018). Application of machine learning to classification of volcanic deformation in routinely generated insar data. *Journal of Geophysical Research: Solid Earth*, *123*(8), 6592–6606.

Banks, D., Davies, C., & Davies, W. (1995). The Chalk as a karstic aquifer: evidence from a tracer test at Stanford Dingley, Berkshire, UK. *Quarterly Journal of Engineering Geology and Hydrogeology*, *28*(Supplement 1), S31–S38.

Bell, J. W., Amelung, F., Ferretti, A., Bianchi, M., & Novali, F. (2008). Permanent scatterer insar reveals seasonal and long-term aquifer-system response to groundwater pumping and artificial recharge. *Water Resources Research*, *44*(2).

Box, G. E., Jenkins, G. M., Reinsel, G. C., & Ljung, G. M. (2015). *Time series analysis: forecasting and control*. John Wiley & Sons.

Brockwell, P. J., & Davis, R. A. (2016). *Introduction to time series and forecasting.* springer.

Burke, H., Hough, E., Morgan, D., Hughes, L., & Lawrence, D. (2015). Approaches to inform redevelopment of brownfield sites: An example from the Leeds area of the West Yorkshire coalfield, UK. *Land Use Policy*, *47*, 21–331.

Carla, T., Intrieri, E., Di Traglia, F., & Casagli, N. (2016). A statistical-based approach for determining the intensity of unrest phases at stromboli volcano (southern italy) using one-step-ahead forecasts of displacement time series. *Natural Hazards*, *84*(1), 669–683.

Chambers, J., Weller, A., Gunn, D., Kuras, O., Wilkinson, P., Meldrum, P., ... others (2008). Geophysical anatomy of the hollin hill landslide, north yorkshire, uk. In *Near surface 2008-14th eage european meeting of environmental and engineering geophysics* (pp. cp–64).

Chen, J., & Boccelli, D. L. (2018). Forecasting hourly water demands with seasonal autoregressive models for real-time application. *Water Resources Research*, *54*(2), 879–894.

Cho, K., Van Merriënboer, B., Gulcehre, C., Bahdanau, D., Bougares, F., Schwenk, H., & Bengio, Y. (2014). Learning phrase representations using rnn encoder-decoder for statistical machine translation. *arXiv preprint arXiv:1406.1078*.

Cleveland, R. B., Cleveland, W. S., McRae, J. E., & Terpenning, I. (1990). Stl: a seasonal-trend decomposition. *Journal of official statistics*, *6*(1), 3–73.

Cleveland, W. S. (1979). Robust locally weighted regression and smoothing scatterplots. *Journal of the American statistical association*, *74*(368), 829–836.

Colesanti, C., Ferretti, A., Novali, F., Prati, C., & Rocca, F. (2003). Sar monitoring of progressive and seasonal ground deformation using the permanent scatterers technique. *IEEE Transactions on Geoscience and Remote Sensing*, *41*(7), 1685–1701.

Crilly, M. (2001). Analysis of a database of subsidence damage. *Structural survey*, *19*(1), 7–15.

Daout, S., Doin, M.-P., Peltzer, G., Socquet, A., & Lasserre, C. (2017). Large-scale insar monitoring of permafrost freeze-thaw cycles on the tibetan plateau. *Geophysical Research Letters*, *44*(2), 901–909.

Gaddes, M., Hooper, A., & Bagnardi, M. (2019). Using machine learning to automatically detect volcanic unrest in a time series of interferograms. *Journal of Geophysical Research: Solid Earth*.

Greff, K., Srivastava, R. K., Koutník, J., Steunebrink, B. R., & Schmidhuber, J. (2017, Oct). Lstm: A search space odyssey. *IEEE Transactions on Neural Networks and Learning Systems*, *28*(10), 2222-2232.

Hamilton, J. D. (1994). *Time series analysis* (Vol. 2). Princeton New Jersey.

Hartmann, D. L., Michelsen, M. L., & Klein, S. A. (1992). Seasonal variations of tropical intraseasonal oscillations: A 20–25-day oscillation in the western pacific. *Journal of the atmospheric sciences*, *49*(14), 1277–1289.

Heleno, S. I., Frischknecht, C., d'Oreye, N., Lima, J., Faria, B., Wall, R., & Kervyn, F. (2010). Seasonal tropospheric influence on sar interferograms near the itcz–the case of fogo volcano and mount cameroon. *Journal of African Earth*

Sciences, *58*(5), 833–856.
Hochreiter, S., & Schmidhuber, J. (1997). Long short-term memory. *Neural Computation*, *9*(8), 1735-1780.
Hylleberg, S. (1995). Tests for seasonal unit roots general to specific or specific to general? *Journal of Econometrics*, *69*(1), 5–25.
Hyndman, R. J., Khandakar, Y., et al. (2007). *Automatic time series for forecasting: the forecast package for r* (No. 6/07).
Kingma, D.-P., & Ba, J. (2015). Adam: A Method for Stochastic Optimization. *International Conference on Learning Representations (ICLR).*
Lake, R., Northmore, K., Dean, M., & Tragheim, D. (1992). Leeds: a geological background for planning and development: 1: 10000 sheets SE23NW, NE, SE and SE33NW, NE, SW, SE: parts of 1: 50000 geological sheets 69 (Bradford), 70 (Leeds), 77 (Huddersfield) and 78 (Wakefield).
Lamont-Black, J., Younger, P. L., Forth, R. A., Cooper, A. H., & Bonniface, J. P. (2002). A decision-logic framework for investigating subsidence problems potentially attributable to gypsum karstification. *Engineering geology*, *65*(2-3), 205–215.
Lazecky, M., Hlavacova, I., Bakon, M., Sousa, J. J., Perissin, D., & Patricio, G. (2016). Bridge displacements monitoring using space-borne x-band sar interferometry. *IEEE Journal of Selected Topics in Applied Earth Observations and Remote Sensing*, *10*(1), 205–210.
Mazzanti, P., Rocca, A., Bozzano, F., Cossu, R., & Floris, M. (n.d.). Landslides forecasting analysis by displacement time series derived from satellite insar data: preliminary results. *Small*, *5000*, 50–000.
McCay, A. T., Valyrakis, M., & Younger, P. L. (2018). A meta-analysis of coal mining induced subsidence data and implications for their use in the carbon industry. *International Journal of Coal Geology*, *192*, 91–101.
Milillo, P., Giardina, G., DeJong, M., Perissin, D., & Milillo, G. (2018). Multi-temporal insar structural damage assessment: The london crossrail case study. *Remote Sensing*, *10*(2), 287.
Rebane, J., Karlsson, I., Denic, S., & Papapetrou, P. (2018). Seq2seq rnns and arima models for cryptocurrency prediction: A comparative study. *SIGKDD Fintech*, *18*.
Rumelhart, D. E., Hinton, G. E., & Williams, R. J. (1986, October). Learning representations by back-propagating errors. *Nature*, *323*, 533–.
Selvakumaran, S., Plank, S., Geiß, C., Rossi, C., & Middleton, C. (2018). Remote monitoring to predict bridge scour failure using interferometric synthetic aperture radar (insar) stacking techniques. *International journal of applied earth observation and geoinformation*, *73*, 463–470.
Sirignano, J., & Cont, R. (2019). Universal features of price formation in financial markets: perspectives from deep learning. *Quantitative Finance*, *19*(9), 1449–1459.
Spaans, K., & Hooper, A. (2016). Insar processing for volcano monitoring and other near-real time applications. *Journal of Geophysical Research: Solid Earth*, *121*(4), 2947–2960.
Sutskever, I., Vinyals, O., & Le, Q. (2014). Sequence to sequence learning with neural networks. *Advances in NIPS*.
Torres, D. G., & Qiu, H. (2018). *Applying recurrent neural networks for multivariate time series forecasting of volatile financial data.* Stockholm: KTH Royal Institute of Technology.
Valade, S., Ley, A., Massimetti, F., D'Hondt, O., Laiolo, M., Coppola, D., ... Walter, T. R. (2019). Towards global volcano monitoring using multisensor sentinel missions and artificial intelligence: The mounts monitoring system. *Remote Sensing*, *11*(13), 1528.
Watson, K. M., Bock, Y., & Sandwell, D. T. (2002). Satellite interferometric ob-

servations of displacements associated with seasonal groundwater in the los angeles basin. *Journal of Geophysical Research: Solid Earth*, *107*(B4).

Zubaidi, S. L., Dooley, J., Alkhaddar, R. M., Abdellatif, M., Al-Bugharbee, H., & Ortega-Martorell, S. (2018). A novel approach for predicting monthly water demand by combining singular spectrum analysis with neural networks. *Journal of hydrology*, *561*, 136–145.